Energy Advances

ROYAL SOCIETY OF CHEMISTRY

PAPER

Published on 23 October 2026
Licensed under CC-BY 4.0

Check for updates

Cite this: DOI: 10.1039/d6ya00228e

Electrochemical intercalation of Na^+ into 1T-HfS_2 – a comparative study using different electrolyte solvents

Lina Liers,[a] Lorena Baumgarten,[bc] Niels Michaelis,[a] Romy Brüning,[a] Henrik Fritzsch,[a] Jan-Dierk Grunwaldt,[bc] Malte Behrens[a] and Sebastian Mangelsen*[a]

Titanium disulfide is a well-known electrode material for batteries and has already been extensively studied for its structural changes during the intercalation of guest ions such as Li or Na. However, the question of how higher homologues, such as HfS_2 – which was investigated in this study – react to the intercalation of Na has remained virtually unexplored. Although all group IV transition metal disulfides (TMDSs) are isostructural and undergo a phase transition from 1T-TMS_2 to 3R-Na_xTMS_2 (TM = Ti, Zr, Hf) during intercalation of sodium ions, the reaction mechanism for each is unique and is influenced by the electrolyte used in the case of electrochemical intercalation. For HfS_2 co-intercalation of both strong and weakly coordinating electrolyte solvents (namely diglyme and an EC:DEC mixture) was investigated by combining XRPD with IR and TG measurements, and only the use of THF shows no evidence of co-intercalation. Furthermore, the intercalation reaction of Na^+ does not occur *via* explicit intermediate structures (TiS_2) or stacking faults (ZrS_2). Instead, phases with different *d*-spacings coexist. The structural studies are complemented with insights in changes of the electronic structure: *in situ* UV/Vis measurements indicate the transformation from a semiconductor to a conducting material during the intercalation of Na^+. X-ray absorption near-edge structure spectroscopy shows only a very small shift of the Hf L_3-edge energy, and EXAFS shows some expansion of the Hf–S atomic distances in $NaHfS_2$ due to the Na^+ intercalation, indicating that sulfur instead of Hf might be involved in the redox process.

Received 24th July 2026,
Accepted 9th October 2026

DOI: 10.1039/d6ya00228e

rsc.li/energy-advances

Introduction

Sodium ion batteries (SIBs) are discussed as abundant and cheap solutions in various fields of rechargeable energy storage devices like portable systems, electric vehicles and grid storages. One aspect that current research focusses on is, whether the co-intercalation of the electrolyte solvent may either enhance or deteriorate the performance of the electrochemical cells.[1–6]

The intercalation reaction of different alkali metals in TiS_2 was shown by several working groups, including the observation of co-intercalation depending on the choice of electrolyte solvent.[7–11] In a previous publication we investigated the intercalation reaction of Na^+ into ZrS_2 by varying the electrolytes, showing that the intercalation of Na^+ causes a phase transition from 1T-ZrS_2 to 3R-$NaZrS_2$. The choice of electrolyte solvent has a decisive influence on the intercalation reaction, particularly on the phase transition. While the strongly coordinating solvent diglyme leads to co-intercalation and thus causes a large expansion of the interlayer distances at low intercalation degrees, there is no evidence of co-intercalation with weaker coordinating solvents such as an EC:DEC mixture or THF. The phase transition, which is induced by stacking faults even at low uptake of Na^+, was investigated in detail.[12] There are no studies on the structural changes during the electrochemical intercalation reaction of sodium into HfS_2.

Although TiS_2 and ZrS_2 are isotypic, the mechanism during Na uptake is different: while TiS_2 undergoes a phase transformation with trigonal prismatic coordination of Na ions (P3) at low Na uptake and an octahedral coordination of Na^+ ion (O3) during the phase transformation of TiS_2 to Na_xTiS_2,[13] ZrS_2 shows only the octahedral coordination of Na^+ ions even at the lowest intercalated amount of sodium ions in the absence of co-intercalation. Furthermore, the intercalation of Na^+ ions into TiS_2 initially runs under structural preservation until an uptake of 0.23 Na^+ per f.u. while ZrS_2 undergoes a direct phase

[a] Institute of Inorganic Chemistry, Christian-Albrecht University of Kiel, Max-Eyth-Str. 2, 24118 Kiel, Germany. E-mail: smangelsen@ac.uni-kiel.de
[b] Institute for Chemical Technology and Polymer Chemistry, Karlsruhe Institute of Technology, Engesserstraße 20, 76131 Karlsruhe, Germany
[c] Institute of Catalysis Research and Technology, Karlsruhe Institute of Technology, Hermann-von-Helmholtz Platz 1, 76344 Eggenstein-Leopoldshafen, Germany

© 2026 The Author(s). Published by the Royal Society of Chemistry

transformation from 1T-ZrS_2 to 3R-$NaZrS_2$.[10,14] This raises the question of whether HfS_2 behaves like ZrS_2 during the uptake of Na^+ ions or shows a different structural response. HfS_2 is isotypic with ZrS_2, crystallizing in the primitively stacked 1T polytype (Ramsdell notation for "1" layer within the unit cell in a trigonal symmetry (T);[15] space group: $P\bar{3}m1$) with a stacking sequence of $AbC[]_TAbC\ldots$, where sulfur atom layers (capital letters) alternating with metal atom layers (lowercase letters) and tetrahedral vacancies are indicated by empty brackets. Within the layers, HfS_6 octahedra are edge sharing where Hf occupies the octahedral sites of hexagonally closed packed sulfur anions. The interlayer distance of the anion layers is 0.59 nm and they are held together by van der Waals forces. The molecular mass of 242.6 g mol^{-1} is about $\frac{2}{3}$ higher than its ZrS_2 analogue (155.4 g mol^{-1}).[16]

Pure HfS_2 is a semiconducting material where s and p orbitals of the sulfur form the valence band and the conduction band is mainly formed by overlapping d orbitals of hafnium.[16,17] Due to its oxidation state +IV hafnium is a d^0 system which means that there are no electrons in the conduction band of HfS_2 and the material is therefore a diamagnetic semiconductor[16–18] with a medium sized band gap of 1.96 eV.[19,20] By the intercalation of sodium into the van der Waals gaps, there is a charge transfer from the electron of the alkali metal to the conduction band of the HfS_2.[17] Meanwhile, the color of the HfS_2 crystals change from red to a metallic sheen.[16] Intercalated HfS_2 shows conducting properties.[17,21]

For the chemical intercalation reaction of lithium into the host structure HfS_2 it is known that the phase transitions from 1T-HfS_2 to 3R-$LiHfS_2$ occur like that of its homologues in group IV. The 3R polytype of $LiHfS_2$ (Ramsdell notation for "3" layers within the unit cell in a rhombohedral symmetry (R); space group: $R\bar{3}m$) is stacked in an $AcB[Li]_OCbA[Li]_OBaC\ldots$ sequence. The Hf ions are octahedrally coordinated by cubic-closed packed sulfur ions. Lithium ions are intercalated in the van der Waals gaps of layers built up from edge-sharing HfS_6 octahedrons. Although $LiHfS_2$ is clearly identified as the 3R phase, the intermediates are coexisting 1T and 3R phases.[10,11,16] There are no studies of the structural changes during the electrochemical intercalation reaction of sodium into HfS_2. We therefore explore this using different electrolyte solvent combinations with varying coordination strengths towards Na^+ of the latter as the focal point of this study and we use X-ray powder diffraction (XRPD) to gain insight into the structural processes. We further combine the studies with chemical analysis, infrared (IR) spectroscopy and thermogravimetry (TG), UV-vis-spectroscopy and X-ray absorption spectroscopy (XAS) for a complete picture. The aim of this study is to find differences and analogies in the reactivity compared to ZrS_2.

Experimental section

Synthesis

The synthesis of HfS_2 was carried out *via* high temperature synthesis: a stoichiometric ratio of hafnium (Haines & Maassen, 99.9%, Zr max. 0.4%) and sulfur (Chempur, 99.999%) was ground and sealed in a quartz glass ampoule ($<10^{-2}$ mbar). The ampoule was placed in a muffle furnace, heated to 723 K with a heating rate of 0.5 K min^{-1}, and maintained at this temperature for 1 d. Afterwards, the temperature was increased to the reaction temperature of 1073 K with a heating rate of 0.7 K min^{-1} and maintained for 3 d.

Electrochemical intercalation

All preparation steps were performed under inert conditions in an argon filled glovebox (99.999% Ar, MBraun Unilab, <1 ppm H_2O, <1 ppm O_2). Around 20 mg of the as-synthesized HfS_2 powder was pressed into pellets with a diameter of 8 mm using a hand press. The obtained pellets with a thickness of $\sim$0.8 mm have an areal loading of 40 mg cm^{-2}. In Swagelok type test cells, the pellets were covered with a separator (Separion S240P30, Litarion) and two glass fiber filters (Whatman™, United Kingdom). Finally, 150 μL 1 M $NaCF_3SO_3$ (NaOTf, abcr, 98%) in bis(2methoxyethyl)ether (Diglyme, Acros Organics, 99+%, extra dry), 1 M $NaC_2HF_6NO_4S_2$ (NaTFSI) in ethylene carbonate and diethyl carbonate (EC : DEC; 1 : 1, solvionic) or 1 M $NaCF_3SO_3$ (NaOTf, abcr, 98%) in tetrahydrofuran (THF, Grüssing, 99% anhydrous) and a punch of pure sodium metal (abcr, 99.95%) as the counter electrode were added. For *in situ* UV/Vis experiments an ECC-Opto-10 test cell (EL-CELL, face-to-face sample holder) was prepared using a punch of pure sodium covered by a glass fiber filter (Whatman™) soaked in 60 μL NaTFSI in EC:DEC or NaOTf in diglyme. The 8 mm pellet of HfS_2 was placed on top of the glass fiber filter. Each experiment was repeated at least three times under similar conditions. The current density varies in between 0.014 and 0.02 A m^{-2}.

A Neware 8 channel battery analyzer was used for galvanostatic cyclisation within a voltage range of 2.8 V to 0.3 V and 2.8 V to 1.0 V respectively, applying a current rate of C/20. The electrochemical reaction was interrupted at different sodium uptake/release steps to investigate the intercalation reaction mechanism. Afterwards, the electrodes were recovered, washed with *n*-hexane and dried in an argon-filled glovebox. The dry powder was filled in borosilicate capillaries and sealed under an argon atmosphere.

Material characterizations

Powder X-ray diffraction (XRPD) was performed in Debye–Scherrer geometry using a PANalytical Empyrean (Cu K_α radiation, λ = 1.54184 Å), focusing X-ray mirror, PIXcel 1-D detector. The samples were loaded in glass capillaries (Spezialglas No. 10, Hilgenberg) of 0.5 mm diameter in an Ar-filled glovebox, with specifications as above. The samples were spun during the measurement to avoid effects of the preferred orientation.

X-ray absorption spectroscopy measurements were performed at the CAT-ACT beamline at the Karlsruhe Institute of Technology (KIT) light source.[22] The XAS data were recorded at the Hf L_3-edge (9560.7 eV) using a Si(111) double-crystal monochromator and the spectra were recorded in transmission mode (step-scans) using ionization chambers for quantification of the

© 2026 The Author(s). Published by the Royal Society of Chemistry

absorption. A reference Zn foil was measured simultaneously with each sample for energy calibration. The raw data were treated using Athena.[23] The edge energies of the spectra were determined using the first maxima in the derivative spectra. For the Zn foil, this maximum was assigned a value of 9658.6 eV. Subsequently, the background was adjusted and the spectra were normalized. The samples were prepared in an argon filled glovebox by grinding and thorough mixing with methyl cellulose, before pressing them into pellets of 100 mg each with a Hf content of about 2 wt%. The pellets were sealed, encapsulated in Kapton foil and measured. HfO_2 was measured accordingly to serve as the reference compound.

For extended X-ray absorption fine structure (EXAFS) analysis, a model was generated from the HfS_2[24] and $NaHfS_2$ (our work) crystal structure using the program Artemis.[23] This model was first fitted to the EXAFS data of the HfS_2 sample in *R*-space to determine the amplitude reduction factor (0.7). Afterwards, the amplitude reduction factor was fixed, and the coordination number was fitted. The same model was applied to the experimental data of $NaHfS_2$. The *k*-window was 3–11 $Å^{-1}$. The fitting range for the Fourier transformed spectra was kept to R = 1.4–2.8 Å with a *k*-weight of 2.

Scanning electron microscopy (SEM) in combination with energy-dispersive X-ray spectroscopy (EDX) was performed on a Hitachi SU8700 equipped with an Oxford EDX detector Ultim 100. The samples were prepared on carbon stripes on an aluminum pin mount sample holder in an argon filled glovebox and transferred to the microscope. Images were recorded using three different detectors, *e.g.* an in-column secondary electron (SE) upper detector (UD), an in-column backscattered electron (BSE) middle detector (MD) and an Everhart–Thornley detector in the chamber (SE/BSE, lower detector LD).

UV/Vis spectroscopy was performed using an Avantes spectrometer with a combination of a AvaSpec-ULS-EVO-RS detector and a AvaLight-DH-S-BAL light source. The measuring range was selected between 200 and 1000 nm. To avoid stray light during measurement, a cap was constructed for the electrochemical cell, which was adapted to the measuring probe. The distance between the probe and the sample was 2 mm. A reference spectrum was recorded using a Whatman in the empty cell. For electrochemical cycling a Biologic VSP potentiostat was used. Cells were cycled between 0.1 and 2.8 V applying a current rate of C/15.

Infrared spectroscopy was performed using a Bruker Vertex 70 FT-IR spectrometer (ATR) equipped with a broadband spectral range extension VERTEX FM for full mid and far IR in the range of 4000–100 cm^{-1}.

Thermogravimetric measurements (DTA/TG) were carried out on a STA PT 1600 and STA 1000 (Linseis Messgeräte GmbH) equipped with a Pt/Rh-thermo couple in flow of 100 sccm N_2. Samples were prepared under inert conditions and transferred in an argon filled crucible.

Crystal structure diagrams were created using Vesta v3.[25]

Results and discussion

Characterization of the pristine sample

HfS_2 was prepared by high temperature synthesis from the elements and characterized *via* XRPD and EDX. XRPD data from the literature matches the observed XRPD pattern and confirms the formation of 1T-HfS_2 (space group $P\bar{3}m1$). A Rietveld refinement (difference plot in Fig. 1a) confirms similar lattice parameters of a = 3.630(5) Å and c = 5.875(3) Å, and a unit cell volume of 67.08(6) $Å^3$ compared to the literature.[24] Despite using the same temperature profile during the synthesis as for ZrS_2, the 00*l* and *h*0*l* reflections are broadened, indicating more stacking faults within the layered structure, which is taken into account in the subsequent consideration of the intercalation reaction of Na^+. A stacking fault analysis using a grid search in Topas[26] shows a transition probability of 8% from layer A to B, whereby layer A and B have identical positions for hafnium and sulfur sites, but layer B has a stacking vector $s_1 = \frac{2}{3}, \frac{1}{3}, 1$ relative to layer A. Other scenarios, such as simple Rietveld refinements with the implementation of preferred orientation were also

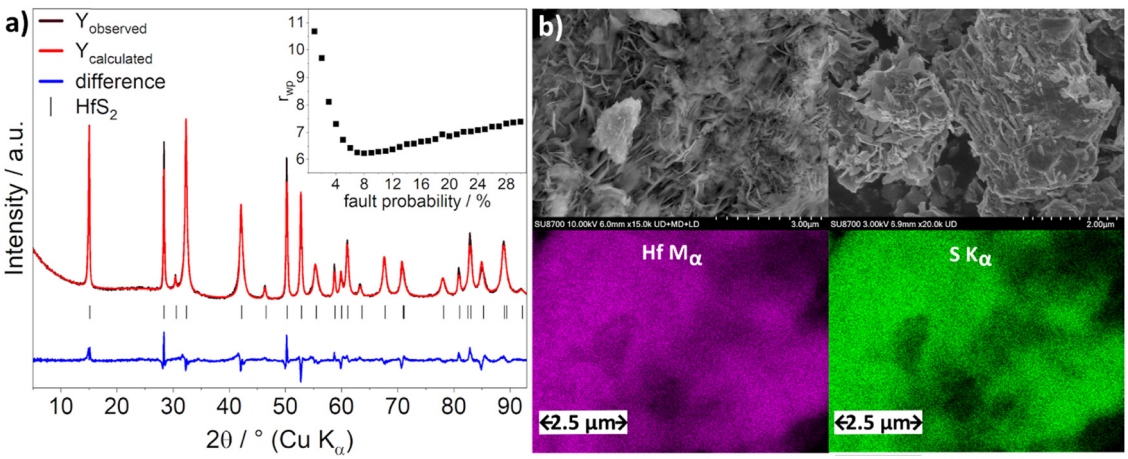


Fig. 1 (a) Difference plot of the Rietveld refinement of HfS_2 obtained from high temperature synthesis with an optimized fault probability of 8%. r_{wp} = 6.2%, GOF = 2.7. The inset depicts the results from a grid search refinement for the transition probability. (b) SEM images of two different particles of the pristine HfS_2 and the corresponding EDX mapping results for Hf (magenta) and sulfur (green) from the top left sample.

© 2026 The Author(s). Published by the Royal Society of Chemistry

considered, but the method shown here yielded the best results. Due to absorption problems an empirical correction was carried out until meaningful displacement parameters were obtained. Nevertheless, some differences in intensities and line shape are observed for the fitted *vs.* the measured pattern. The mismatch is not due to preferred orientation and is thus regarded as due to results from other types of stacking faults, but this is not investigated further. EDX results also confirm the composition of HfS_2 and the distribution of sulfur and hafnium is uniform (Fig. 1b). SEM images show agglomerates of varying sizes showing mostly a thin, plate-like morphology.

Electrochemical analysis of the intercalation reaction

HfS_2 was examined with regard to its electrochemical intercalation of Na^+ ions using electrolytes differing in particular in the coordination strength of the solvent, namely 1 M NaTFSI in EC:DEC, 1 M NaOTf in THF and 1 M NaOTf in diglyme were used. Both salts exhibit similar electrochemical properties, and have the same decomposition products. Nevertheless, during solid electrolyte interphase (SEI) formation, OTf^- exhibits poorer properties than $TFSI^-$. The oxidation potentials are >3.5 V.[27–29] However, since we will not be investigating SEI formation further and the oxidation potentials lie outside of our voltage range, the following article will focus only on the different solvents. The voltage profiles provide initial indications of the course of the intercalation reaction, where steps or discontinuities indicate phase transitions or ordering processes, while plateaus indicate a two-phase region where different phases coexist.[13,30,31] The voltage profiles of the first discharge using the electrolytes 1 M NaTFSI in EC:DEC and 1 M NaOTf in THF are similar and show only one voltage plateau at 1.26 V and 1.48 V, respectively. In contrast, the profile using 1 M NaOTf in diglyme differs in that two voltage plateaus are observed at 2.1 V and 1.1 V (Fig. 2a). From previous work on the intercalation of Na^+ in ZrS_2, it can be deduced that the plateau at 2.1 V is likely a co-intercalation of diglyme molecules.[8,12] It is also noticeable that nominally 1.2 Na^+ per f.u. can be intercalated using 1 M NaTFSI in EC:DEC and 1.8 Na^+ per f.u. for 1 M NaOTf in diglyme, while the expected 1 Na^+ per f.u. (filling of all octahedral voids in 3R-$NaHfS_2$) is intercalated when using 1 M NaOTf in THF. It can be assumed that at low potentials, the electrolyte on the electrode surface decomposes, allowing a larger amount of charge to be passed due to this side reaction, which is not to be mistaken for an intercalation beyond the limit of 1.0 Na^+ per f.u. Furthermore, a coloration of the separator was observed for high intercalation degrees, which could be an indication of a formation of sodium polysulfides (Na_xS_y) caused by a conversion reaction of Na_xHfS_2. However, there is no further analytical evidence of polysulfide formation. The voltage profiles of the first charge (Fig. 2b) using 1 M NaTFSI in EC:DEC and 1 M NaOTf in THF show an almost identical trend. However, up to an uptake of 0.6 Na^+ per f.u., the voltage profiles show a continuous slope, and only after that a brief plateau can be observed at 1.65 V. Using 1 M NaTFSI in EC:DEC, only 0.9 Na^+ per f.u. is nominally released and by using 1 M NaOTf in THF, we were unable to fully charge the battery cell in any of the experiments. Therefore, no conclusions can be drawn regarding the amount of Na^+ released. As with the discharge process, the voltage profile differs when 1 M NaOTf in diglyme is used. Changes in the profile are only slightly noticeable, and the voltage rises steadily until a release of 1.06 Na^+ per f.u.

In order to gain insight into the structural changes during intercalation of Na^+ into the HfS_2 host structure, *ex situ* XRPD measurements were carried out, the results of which are discussed in the following paragraph. One has to keep in mind that we use the calculated Na^+ uptake from the obtained specific capacities throughout the article. Only random samples of $Na_{0.14}HfS_2$, $Na_{0.45}HfS_2$, $NaHfS_2$ and HfS_2 were used to investigate the compositions *via* EDX measurements.

Using diglyme as the electrolyte solvent

To analyze potential phase transitions during Na^+ intercalation we performed *ex situ* XRPD measurements of samples at a

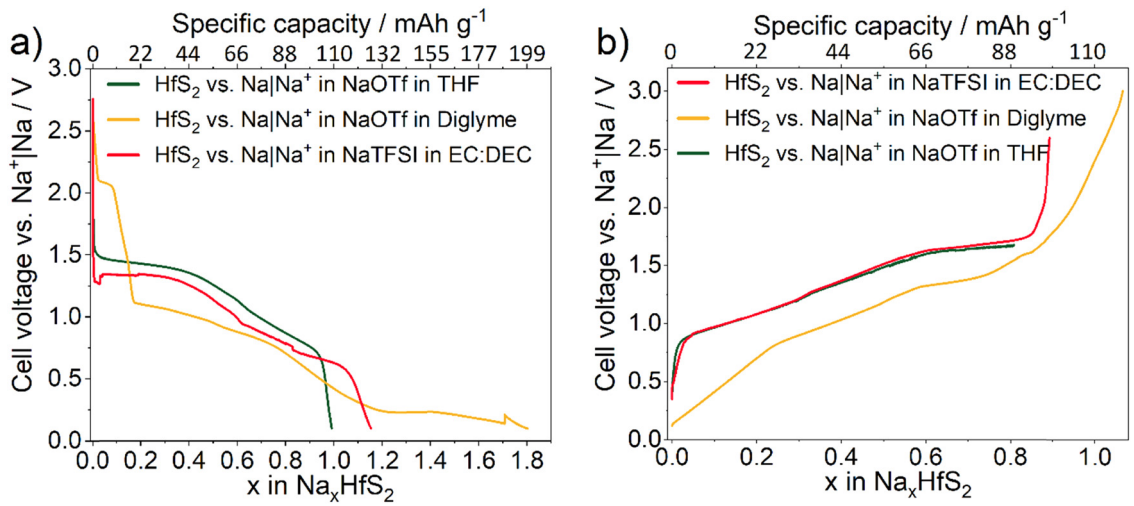


Fig. 2 Voltage profiles of the first discharge (a) and charge (b) of HfS_2 *vs.* $Na^+|Na$ cells using THF (green), diglyme (yellow) and EC:DEC (red) as electrolyte solvents.

© 2026 The Author(s). Published by the Royal Society of Chemistry

defined uptake and release of Na^+ ions at points indicated in Fig. 3a, and the XRPD data are presented in Fig. 3b. The intercalation of 0.14 and 0.27 Na^+ per f.u. into 1T-HfS_2 using a diglyme based electrolyte results in diffraction patterns showing reflections of high intensity at 6.1° (d = 14.4 Å), 12.3° (d = 7.2 Å) and 18.5° 2θ (d = 4.8 Å) which indicates a large volume expansion along the c-axis and can be assigned to a co-intercalated $Na_xHfS_2{\cdot}x$ diglyme phase with tentative Miller indices of 001, 002 and 003 respectively in line with the d-spacings being corresponding fractions. The co-intercalation of diglyme molecules was observed before for the intercalation of Na^+ in TiS_2 and ZrS_2 using diglyme based electrolytes.[8,12] At an uptake of 0.14 Na^+ per f.u., the 001 reflection of the 1T-HfS_2 phase is still observable, whereas after an uptake of 0.27 Na^+ per f.u., this reflection disappeared, but other reflections of the 1T-HfS_2 phase can still be observed at diffraction angles >25° 2θ. By further intercalation, reflections indicating the co-intercalation disappear and only reflections of 3R-Na_xHfS_2 can be observed. Conspicuously, the 00l reflections are initially of weak intensity, virtually merging with the background at an uptake of 0.6 Na^+ per f.u. and appearing as two reflections at 11.8° and 13.2° 2θ after an uptake of 0.7 and 0.9 Na^+ per f.u., indicating coexisting structural domains with different d-spacings. It is noticeable that the reaction continues for $x > 1$, which either indicates a higher specific capacity of HfS_2 or a side reaction of the electrolyte that already begins at $x < 1$. Even after a charge uptake that would correspond to 1.36 Na^+ per f.u., the 003 reflection shows a split peak shape proposing that the Na^+ ions have not yet been evenly distributed and the layers are still unevenly occupied corresponding to slight differences in the d-spacings. In comparison, the d-spacings are smaller than at low uptake of Na^+ ions. The split peak shape can be caused by at least two different domain types with different amounts of intercalated Na^+. Furthermore, the d-values are between the initial values of 1T-HfS_2 and 3R-$NaHfS_2$. After an uptake of nominal 1.8 Na^+ per f.u. the 003 reflection is symmetric yet fairly broad, and all reflections can be assigned to 3R-Na_xHfS_2 with lattice parameters of a/b = 3.624(9) Å, c = 20.42(2) Å and a cell volume of 232.3(9) Å^3, which was refined using the structure model of 3R-$NaZrS_2$.[12] However, reflections remain broadened, but the 101 and 110 reflections appear to be slightly less broadened, indicating structural disorder of the layers relative to each other caused by the large expansion of the interlayer spacings during co-intercalation and its collapse during deintercalation of the solvent molecules. Additionally, some disorder may be inherited from the stacking disorder of the pristine material.

After deintercalation of Na^+ the XRPD pattern shows the same reflection positions as for low Na^+ uptake, but the reflections are broadened, and some exhibit an anisotropic peak shape (Warren type) meaning that the layer spacing is expanded again by the co-intercalation of diglyme molecules and the layers are turbostratically disordered.[32] In line with the voltage profile, this is a strong indication that Na^+ cannot be completely deintercalated from the layers.

One has to keep in mind that in this data set a maximum uptake of 1.8 Na^+ per f.u. is measured which is almost double of the maximum theoretical uptake of 1 Na^+ per f.u. This can be caused by the formation of a SEI which results from the decomposition of the electrolyte within the first discharge. Within following cycles the specific capacity decreases, *i.e.* the maximum amount of intercalated Na^+ per f.u. decreases, until the theoretical specific capacity of 110 mAh g^{-1} is reached after the 10th cycle. The specific capacity then continues to decrease until it stabilizes at 40 mAh g^{-1} (Fig. S1). This rapid and continuous fading capacity is caused by the large volume changes during the (co-)intercalation reaction. The combination from the phase transition from 1T-HfS_2 to 3R-$NaHfS_2$

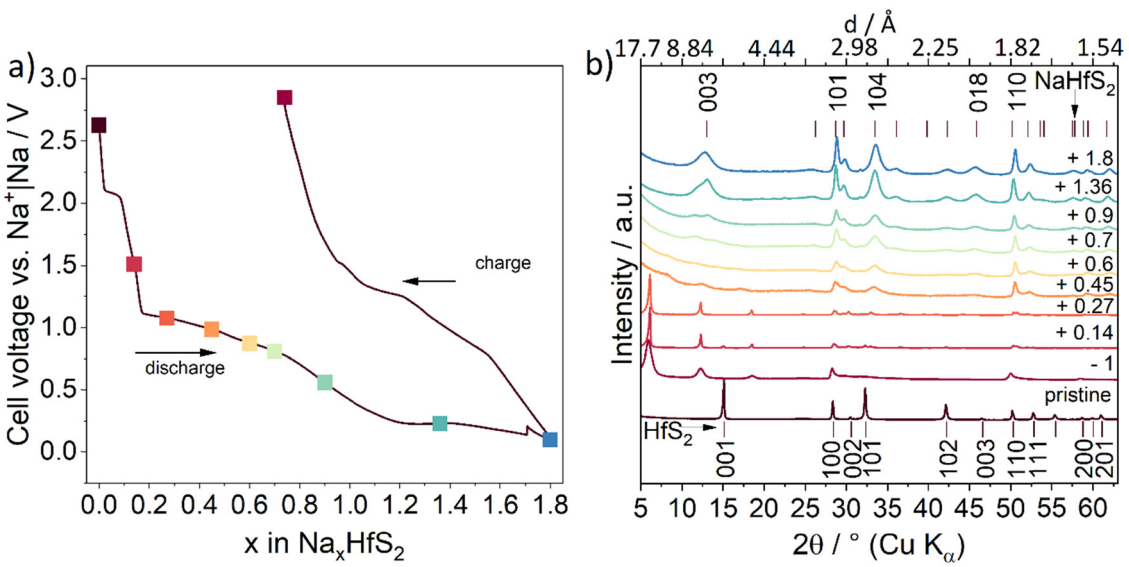


Fig. 3 (a) Voltage profile of the first cycle HfS_2 *vs.* Na^+|Na using a diglyme-based electrolyte. (b) *Ex situ* XRPD patterns collected at different points of intercalation which are marked with colored squares in (a) with the uptake of Na^+ per f.u. as indicated.

© 2026 The Author(s). Published by the Royal Society of Chemistry

(and back) during each (de)-intercalation and the observed incomplete deintercalation of Na^+ and re-co-intercalation of diglyme exerts massive stress on the structure, leading to increasing degradation after several cycles.

Using EC DEC and THF as the electrolyte solvent

The following section compares results from HfS_2 *vs.* $Na^+|Na$ cycled with an EC:DEC mixture and THF as the electrolyte solvent, which we discuss side by side given the similarities.

The voltage profiles of cells cycled using EC:DEC (Fig. 4a) or THF (Fig. 4c) based electrolytes are similar in that only a single plateau at 1.3 V and 1.48 V, respectively can be observed in the first discharge. The first difference, however, is that cells cycled using an EC:DEC based electrolyte can formally intercalate 1.15 Na^+ per f.u. during the first discharge, whereas cells cycled with a THF based electrolyte can formally intercalate 1 Na^+ per f.u. During the charging process of the cells using EC:DEC based electrolyte, a complementary curve can be observed. However, according to the voltage profile, still 0.1 Na^+ per f.u. is intercalated after charging, which is consistent with the broadened reflections and a slight asymmetry of the reflection profile. When using the THF based electrolyte, only incomplete charging curves could be obtained because the cells cannot be sealed tightly enough and the THF completely evaporates during charging.

The XRPD patterns are similar, though slight differences in the reflection profiles can be observed. When using EC:DEC as the electrolyte solvent (Fig. 4b), the XRPD patterns match

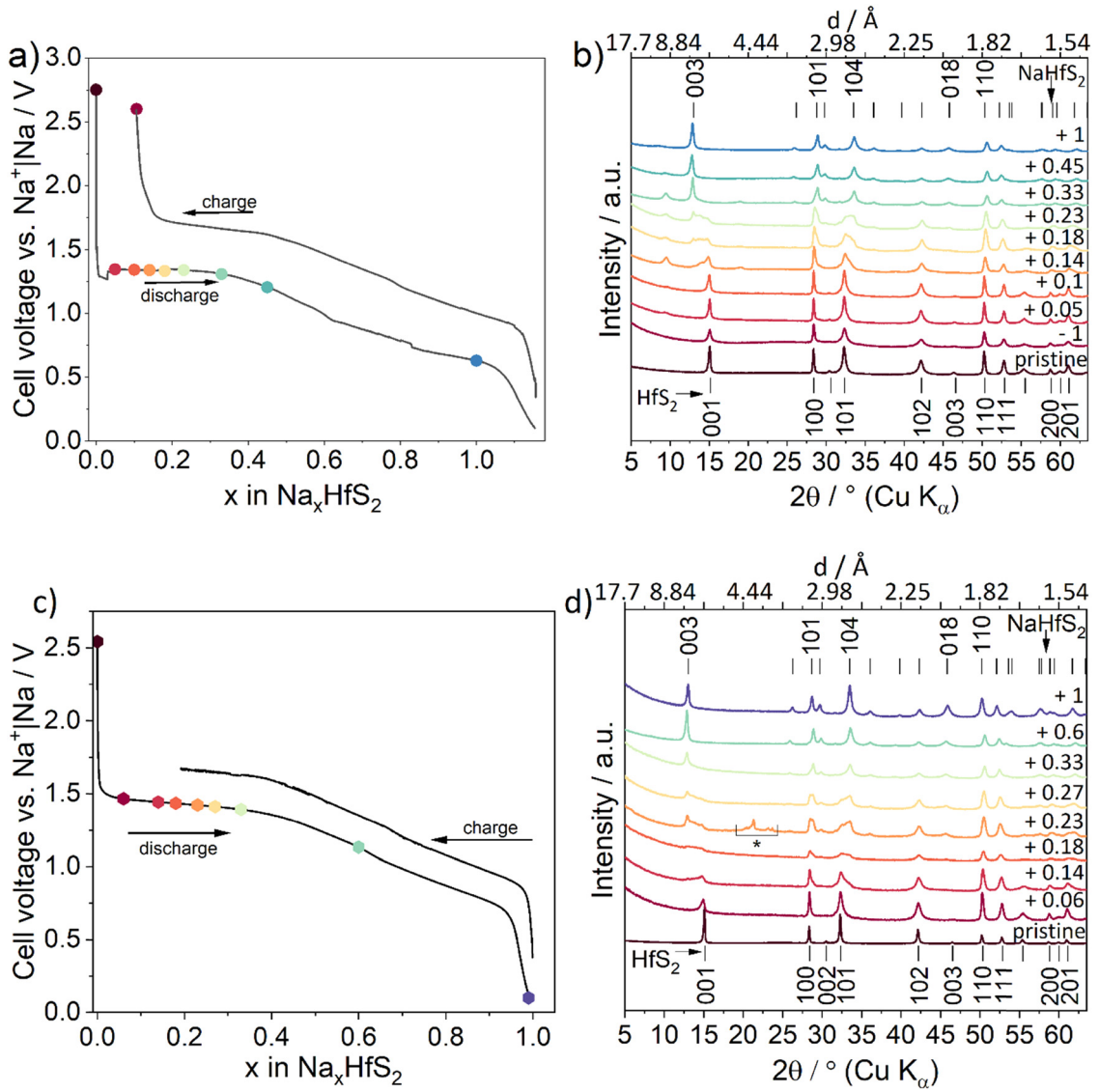


Fig. 4 (a) First cycle voltage profile of HfS_2 *vs.* $Na^+|Na$ using NaTFSI in EC:DEC and colored dots which mark the termination points of the intercalation reaction at which *ex situ* XRPD (b) data were recorded, with the uptake of Na^+ per f.u. as indicated. (c) Voltage profile of HfS_2 *vs.* $Na^+|Na$ using THF as the electrolyte solvent. Colored hexagons mark points where the intercalation reaction was interrupted and *ex situ* XRPD was performed with the uptake of Na^+ per f.u. as indicated. Patterns are shown in (d). Reflections marked with an asterisk are caused by the separator which could not be completely removed during the washing process.

© 2026 The Author(s). Published by the Royal Society of Chemistry

1T-HfS_2 and only slight changes in the reflection positions can be observed until an uptake of 0.1 Na^+ per f.u., while when using THF (Fig. 4d) as the electrolyte solvent an asymmetry of the 001 reflection to smaller diffraction angles and of the 10*l* reflections to higher diffraction angles are observed (Fig. 4d). At higher degrees of intercalated Na^+ (0.14 Na^+ per f.u.) the XRPD patterns of cells cycled using EC:DEC and THF based electrolytes show the same trend as the 001 reflection split into at least two reflections with the highest intensity at 14.9° 2θ, the 100 reflection at 28.4° 2θ and 101 reflection at 32.4° 2θ show an asymmetric peak shape and the 110 reflection at 50.4° 2θ shifts towards higher diffraction angles, indicating a slight expansion of the interlayer spaces and a contraction of the layers itself (Fig. S2). After an uptake of 0.18 and 0.23 Na^+ per f.u. the 00*l* reflection splits into three reflections of low intensity and the 101 reflection splits into at least two reflections (Fig. S3), indicating the presence of domains with different *d*-spacings and thus different concentrations of intercalated Na^+. The three reflections (00*l*) can be assigned to coexisting 1T-HfS_2, 3R-$NaHfS_2$ and a Na_xHfS_2 phase with different *d*-spacings. Furthermore, the reflection at 28.4° 2θ shows a split peak shape into two reflections at the position of the 100 (28.4° 2θ) of 1T-HfS_2 and 101 reflection of 3R-$NaHfS_2$ (28.9° 2θ). From an uptake of 0.33 Na^+ until 1 Na^+ per f.u. the reflections sharpen and can be assigned to 3R-Na_xHfS_2. An interesting detail is that when using EC:DEC as the electrolyte solvent, the 110 reflection continues to shift to higher diffraction angles until an uptake of 1 Na^+ per f.u. The lattice parameters change slightly in that *a* and the cell volume increase and *c* decreases (Table S2). The lattice parameters obtained from Pawley fits for $NaHfS_2$ using THF as the electrolyte solvent are *a*/*b* = 3.631(6) Å, *c* = 20.33(6) Å and a cell volume of 232.2(8) $Å^3$ and using EC:DEC as the electrolyte solvent are *a*/*b* = 3.604(0) Å, *c* = 20.54(2) Å and a cell volume of 231.0(7) $Å^3$. If we assume that the lattice parameters obtained from the Pawley refinements of the samples using THF as the electrolyte solvent are intrinsic to Na_xHfS_2 (with *x* = 1), since the XRPD patterns show no evidence of side phases, then the lattice parameters for the samples with EC:DEC correspond to an uptake of ~0.6 Na^+ per f.u., and those for the sample with diglyme correspond to an uptake of ~0.8 Na^+ per f.u. The fact that the 110 reflection in the XRPD pattern of the sample with EC:DEC does not shift to its theoretical position but continues to shift toward higher diffraction angles, together with the remaining additional reflections in the XRPD pattern, indicates that solvent molecules are co-intercalated in the interlayer spaces, causing a contraction along the *a*/*b* axis.

After the deintercalation of Na^+, reflections can be assigned to 1T-HfS_2, but some line broadening indicates more pronounced structural disorder compared to the even distorted pristine material. This could be related to the larger volume expansion caused by a co-intercalation of EC and/or DEC solvent molecules during the discharge of the cell or the incomplete deintercalation of Na^+. However, since no pronounced expansion along the *c* axis can be observed in contrast to when diglyme is used, the XRPD pattern provides no indication of co-intercalation in this state of charge.

The main difference between the XRPD patterns of samples that were intercalated using EC:DEC instead of a THF based electrolyte is the additional reflections at 9.5 (*d* = 9.3 Å) and 19.05° 2θ (*d* = 4.65 Å). The *d*-spacings are integer multiples of each other which leads to the assumption that the reflections correspond to a new 00*l* series, as we have already observed by using diglyme as the electrolyte solvent to intercalate Na^+ into 1T-HfS_2, but here the expansion of the interlayer spaces is less pronounced (9.3 *vs.* 14.3 Å). Assuming a HfS_2 layer thickness (derived from the *z*-components of the sulfur atoms in the crystal structure) of 3 Å, the samples treated with the EC:DEC electrolyte retain an interlayer distance of 6.3 Å, which corresponds to the size of the solvation shell EC or DEC forms with sodium.[8,33] Therefore, it is assumed that EC and/or DEC are also co-intercalated between the HfS_2 layers. In contrast to the co-intercalation of diglyme, the reflections – albeit of lower intensity – are still observable in the patterns up to complete intercalation. This could also explain the differing lattice parameters when using EC:DEC as the electrolyte solvent in that the solvent molecules occupy lattice sites that could otherwise be occupied by sodium, which explains the lower value for *a* and the higher value for *c*. Furthermore, it could be an explanation for the voltage hysteresis between the end of the discharge and the beginning of the charge. To identify the origin of the additional reflections IR (Fig. S4) and TG (Fig. S5) measurements were performed to check whether a co-intercalation of EC and/or DEC occurs. The samples after an uptake of 0.14 and 0.45 Na^+ per f.u. show IR active bands at 1130 and 980 cm^{-1} which are in good agreement with the bands of the electrolyte for C═O stretching vibrations. After an uptake of 1 Na^+ per f.u. only faint bands are observable in the corresponding wavelength range. Furthermore, the TG curves for all samples show a total mass loss of 12–14% (0.45 Na^+, 1 Na^+, 0.14 Na^+) in the temperature range up to 800 °C. Two distinct mass loss steps at peak temperatures of 129.15 °C (5.6%) and 362.85 °C (6.7%) were observed for the sample intercalated with 0.14 Na^+ per f.u. The first step can be assigned to the boiling point of diethyl carbonate (125 °C) and the second step could be caused by the reaction of residual moisture or oxygen from the inert gas stream with $NaHfS_2$ combined with the evaporation of ethylene carbonate (boiling point: 248 °C). As the degree of intercalation increases, the first stage of mass loss becomes progressively smaller (2.4% at 177.05 °C for $Na_{0.45}HfS_2$; 1.11% at 189.15 °C for $NaHfS_2$) and shifts to higher temperatures. At the same time, the second mass loss step is more likely split into two steps with a total mass loss of 10.6% at 300.35 °C and 353.65 °C for $Na_{0.45}HfS_2$ and with a total mass loss of 7.19% at 302.25 °C and 374.55 °C for $NaHfS_2$. In conclusion a co-intercalation of the carbonates between the layers of HfS_2 is conceivable. Since the two carbonates are too similar in IR spectroscopy, it cannot be said with certainty whether only one of the two carbonates is co-intercalated or both. Nevertheless, based on the different boiling points indicated in the TG data, it can be concluded that the electrolyte residues are most likely diethyl carbonate. EDX measurements and mapping confirm the composition of $Na_{0.14}HfS_2$, $Na_{0.45}HfS_2$ and $NaHfS_2$. Furthermore, a uniform

© 2026 The Author(s). Published by the Royal Society of Chemistry

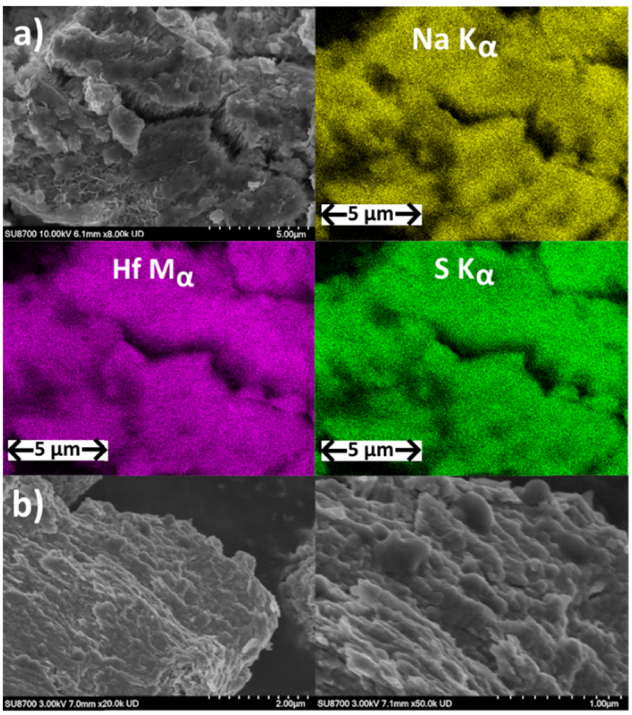


Fig. 5 (a) EDX mapping and the corresponding SEM image of a fully intercalated $NaHfS_2$ sample with the distributions of Na (yellow), Hf (magenta) and S (green). (b) SEM image with a detailed view on the particle edge of a $NaHfS_2$ particle.

distribution of Hf, Na and S can be observed in the EDX mapping (Fig. 5 and Fig. S6 and S7). In addition, an even distribution of F can be observed in the EDX mapping, which can only be attributed to residues of the electrolyte salt. Possible causes for the detectable amount of F include an incomplete washing process during sample preparation or the formation of a SEI. One has to keep in mind that the decomposition of SEI residues adhering to the surface can also affect mass loss on the TG curve. Furthermore, there is no evidence of co-intercalation of EC or DEC in other studies. When sodium is intercalated into graphite, only the co-intercalation of ethers in corresponding electrolytes has been observed to date.[1,2,8,34,35] In conventional batteries, EC is often used as a part of the electrolyte because it contributes to the formation of a stable SEI and thus protects graphite, in particular, from the co-intercalation of solvent molecules.[36,37] In HfS_2 this SEI does not appear to form sufficiently from EC, which allows the co-intercalation of solvent molecules that have a structural effect in the intercalated Na_xHfS_2. A detailed discussion of the composition of the SEI or its formation on HfS_2 would go beyond the scope of this work and will therefore not be addressed further.

The previous results of using THF and EC:DEC as electrolyte solvents show that for low intercalation degrees only slight changes of the 1T-HfS_2 structure are observable but with increasing amount of intercalated Na^+ there is a mixture of 1T-HfS_2, 3R-$NaHfS_2$ and Na_xHfS_2 phases with different interlayer spacing. When the structure is filled by 1/3 f.u. of Na^+, solely 3R-Na_xHfS_2 is observed. Besides the co-intercalation of diglyme and DEC molecules, the intercalation reaction of Na^+ into 1T-HfS_2 is comparable using different electrolytes. The intercalation of Na^+ seems to be hindered, causing a less pronounced order of the structures and therefore coexisting 1T-HfS_2 and 3R-Na_xHfS_2 domains indicated by the split of the 00*l*, 101 and 201 reflections.

To put these results into context, they are compared with our previous findings on the intercalation of Na^+ in 1T-ZrS_2.[12] When using EC:DEC as the electrolyte solvent the *ex situ* XRPD patterns of 1T-ZrS_2 show a continuous transformation between 1T-ZrS_2 and 3R-$NaZrS_2$ in which the reflections shift from the initial to the final position and the phase transition is induced by stacking faults. In contrast, for HfS_2 *ex situ* XRPD patterns show reflections which can be assigned to 1T-HfS_2 after an uptake of up to 0.1 Na^+ per f.u. At higher degrees of intercalated Na^+ per f.u., the 00*l*, 101 and 201 reflections show a split peak shape which can be assigned to 1T-HfS_2, 3R-$NaHfS_2$ as well as a Na_xHfS_2 phase with an intermediate *d*-spacing. In general, the reflections in the XRPD patterns of $(Na)_xHfS_2$ are broadened and even the synthesized sample of HfS_2 has stacking faults. It is important to keep in mind that stacking faults that arise during synthesis can influence the diffusion pathways within the HfS_2 layers and can therefore affect the structural changes that occur during Na^+ intercalation. Furthermore, reflections of a new 00*l* series indicates that EC and/or DEC molecules are co-intercalated which is less pronounced in the XRPD patterns of $(Na)_xZrS_2$. There was only one pattern of $Na_{0.06}ZrS_2$ with one additional reflection at a similar position (9.7° 2θ) of which the origin remained unclear. These results suggest that the intercalation reaction is more kinetically hindered than in ZrS_2, which may be intrinsic to the compound or related to a higher stacking fault density within the pristine 1T-HfS_2 which can cause a sluggish phase transition within these faulted layers. The energetics of stacking faults may be slightly different in HfS_2 compared to ZrS_2 which would explain both the higher fault density in the pristine material but also the sluggish transition during electrochemical intercalation.

Both compounds exhibit reflections in the XRPD patterns which indicate co-intercalation of diglyme up to an uptake of 0.3 Na^+ per f.u. In contrast, for Na_xZrS_2 reflections can be assigned to 3R-Na_xZrS_2 after an uptake of 0.6 Na^+ per f.u. whereas for Na_xHfS_2 an amount of $x > 1$ Na^+ per f.u. has to be intercalated that the reflection positions fit solely 3R-Na_xHfS_2.

UV-Vis-spectroscopy

Since HfS_2 exhibits a change in its optical properties during intercalation of Na^+, we investigated this using *in situ* UV/Vis spectroscopy. To the human eye, a color change of the powder electrode from orange (HfS_2) to dark blue ($NaHfS_2$) was observed (Fig. S8). *In situ* UV/Vis spectroscopy was performed to analyze the optical and electronic changes by intercalating Na^+ into 1T-HfS_2 to form 3R-$NaHfS_2$ in detail. It was compared if the choice of electrolyte solvent has any influence on the starting time of the transition. Unfortunately, NaOTf in diglyme shows an absorption band from 250–300 nm which overlaps with an absorption band of HfS_2 (Fig. S9). Nevertheless, for the

© 2026 The Author(s). Published by the Royal Society of Chemistry

first 75 min a shift of the absorption band from 300 to 330 nm (diglyme; Fig. 6a and b) and from 430 to 475 nm (EC:DEC; Fig. 6c and d) is detectable, which corresponds to an uptake of ~0.1 Na^+ per f.u. This absorption band starts to shift back to the initial wavelength within the following 425 min while the formation of a new absorption band in the IR region can be observed. For cells using diglyme as the electrolyte solvent, the band starts to form from 330 min which corresponds to an uptake of ~0.38 Na^+ per f.u. and for cells using EC:DEC as the electrolyte solvent the formation of the band starts after 350 min which corresponds to an uptake of 0.4 Na^+ per f.u. (Fig. 6 and Fig. S10). This band broadens and grows in intensity until the end of the discharge, *i.e.* the end of the intercalation reaction. The results correlate with the results from XRPD data in that the formation of the absorption band starts when the phase transition from 1T-HfS_2 to 3R-Na_xHfS_2 ended and the increase of intensity correlates with the continued intercalation of Na^+ into 3R-Na_xHfS_2. Furthermore, the reductive signals in the dQ/dV plot correspond to the changes in the spectra (Fig. S8; inset). This is in accordance with the transition from a medium-to-large band gap semiconductor to a conductor. The pristine 1T-HfS_2 is a d^0 diamagnetic semiconductor, where s and p orbitals from sulfur form the valence band and the conduction band is mainly formed by the overlap of d orbitals of hafnium.[16,18,19] When sodium is intercalated, an electron is added to the conduction band. The optical behavior of intercalated HfS_2 was already observed in 1981 by Beal and Nulsen for the Li analogue.[21] Following the intercalation of Li^+, a shift of the absorption bands at 326–495 nm toward shorter wavelength was also observed, as well as the formation of a new absorption band starting at 620 nm and extending into the IR region.

X-ray absorption spectroscopy

Since we now know from XRPD and optical measurements there are structural and electronic changes during the intercalation reaction between Na and HfS_2 to form $NaHfS_2$, the question raises if there is a change in formal oxidation state on Hf from +IV to +III due to a redox process. To probe this, XAS measurements at the Hf L_3-edge were performed. In the near-edge absorption spectra (XANES), a shoulder compared to HfO_2 is observed around 9570 eV, typical for HfS_2. Similar features

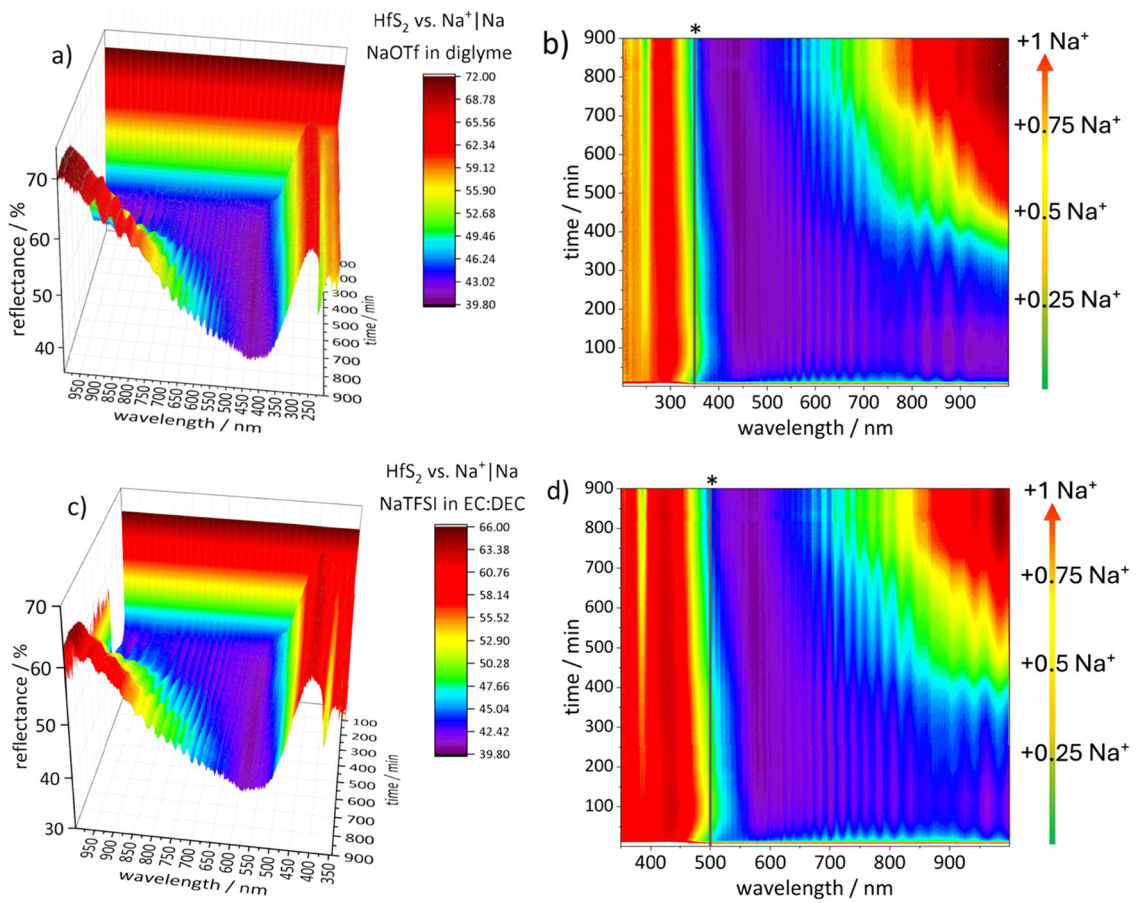


Fig. 6 *In situ* UV/Vis spectra during the first discharge of HfS_2 *vs.* Na^+|Na using diglyme (a/b) and EC:DEC (c/d) as electrolyte solvents. In (a) and (c) 3D plots show a time-resolved change in the absorption bands during the intercalation of Na^+ and for a better visibility of the absorption band shifts a contour plot is shown in (b) and (d) in which the grey line marked with an asterisk is placed as a guidance and an arrow with the corresponding uptake of Na^+ per f.u. is shown on the right-hand side. The wave-like background is caused by some uneven scratches on top of the reflection mirror within the optical cell.

© 2026 The Author(s). Published by the Royal Society of Chemistry

Table 1 Comparison of the near-edge absorption energies as well as the bond length obtained from EXAFS and Rietveld refinements of HfS_2 and $NaHfS_2$. Details on the EXAFS analysis are provided in Fig. S11 and Table S3

	Near-edge absorption energy (eV)	Bond length (Å) Hf–S from EXAFS	Bond length (Å) Hf–S from Rietveld
HfS_2	9559.8	2.54	2.53
$NaHfS_2$	9560.2	2.56	2.58

and absorption energies are observed for HfS_2 and $NaHfS_2$ (9559.8 and 9560.2 eV, respectively, Table 1, Fig. 7a). The Hf L_3-absorption edge of HfO_2 lies at slightly higher absorption energies (9561.0 eV) which is related to the higher electronegativity of oxygen compared to sulfur.[38] The data does not indicate a reduction of Hf^{4+} in $NaHfS_2$, as in this case a significantly larger shift of the absorption towards lower energy would be expected. Thus Hf^{4+} does not seem to be the redox active species during the intercalation reaction of Na^+. In comparison, the intercalation reaction of Na^+ into TiS_2 is indicated by a shift of the absorption edge towards lower energy as Ti^{4+} is reduced to Ti^{3+}.[39]

In the XANES spectra the intensity of the white line of HfS_2 is slightly higher compared to $NaHfS_2$ (Fig. 7a), which could be related to a change of the orbital energies by the intercalation of Na^+ in HfS_2.[40] For EXAFS analysis, the obtained data were Fourier-transformed and the resulting pseudo-radial distribution function (pRDF) is shown in Fig. 7b. The corresponding k^2-weighted EXAFS $\chi(k)$ spectra and the FT window are shown in Fig. S11. In comparison, the peaks of the first shell are of less intensity in the pRDF after the intercalation of Na^+. Furthermore, a slightly lower coordination number of Hf–S (1.0 ± 0.1) in $NaHfS_2$ is observed compared to HfS_2 (0.9 ± 0.1) based on the fitting of the first shell (Table S3) in agreement with the shift of the backscattering peak in Fig. 7b. This and the elongated Hf–S bond length in $NaHfS_2$, which is consistent with the results from Rietveld refinement (Table 1), indicate that Na^+ intercalation induce an expansion of the HfS_2 structure, similar to the effect of Na^+ intercalation into TiS_2.[39] With no evidence of Hf reduction, it is likely that sulfur is involved in the redox process during intercalation of Na^+. A similar observation for anionic redox processes in TMDCs was already made.[41] In addition, it had already been observed earlier that during wet chemical intercalation using *n*-butyl lithium of Li in TiS_2 the electrons are shared between Ti and S.[42] To prove this hypothesis, XAS measurements at the S K-edge would be necessary and are planned for future work.

Conclusion

Just as for ZrS_2, the intercalation of Na^+ into HfS_2 also results in a phase transition from 1T-HfS_2 to 3R-$NaHfS_2$, although this process is characterized by more sluggish kinetics compared to the intercalation of Na^+ into ZrS_2. But this could also result from the higher initial defect density in the pristine HfS_2 compared to pristine ZrS_2 as more stacking faults hinder the Na^+ diffusion within the layers of HfS_2. Furthermore, the use of diglyme as the electrolyte solvent results in an expansion of the interlayer space, indicating co-intercalation as was also observed for ZrS_2. However, a larger uptake of Na^+ is necessary to form 3R-Na_xHfS_2. Surprisingly, there is an indication of co-intercalation of the carbonate mixture (EC:DEC), a phenomenon that had not previously been reported in the intercalation reaction of Na^+ into either TiS_2 or ZrS_2. Therefore, it is worthwhile to critically consider analogies when working with higher homologues, as expectations like reaction mechanisms or kinetics may deviate from the empirically obtained results. Furthermore, in this study we were able to demonstrate that XAS measurements revealed no significant charge transfer from hafnium, but UV/Vis data indicate metallization due to the intercalation of Na^+ into HfS_2. Since an electron transfer is essential for electrochemical intercalation reactions, we suspect that sulfur is the redox active species in this compound. This contrasts with the classical picture of an ionic compound,

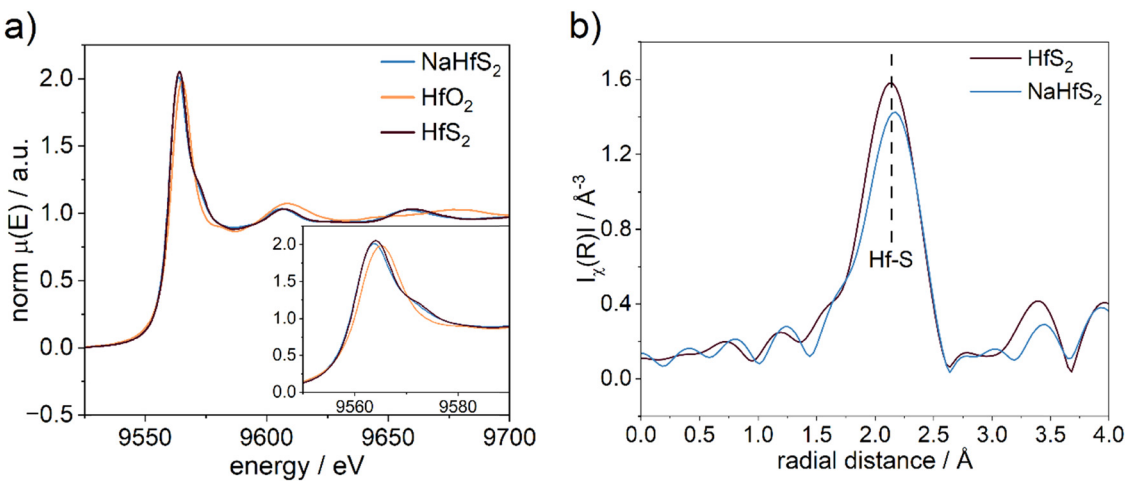


Fig. 7 (a) XANES spectra of $NaHfS_2$, HfS_2 and HfO_2 at the Hf L_3 edge. The inset depicts a closer view of the absorption edge. (b) Radial distribution distances for Hf absorber atoms of HfS_2 and $NaHfS_2$.

© 2026 The Author(s). Published by the Royal Society of Chemistry

in which a formal charge transfer to the metal would be expected. Hence, this study emphasizes the importance of investigating the reaction mechanism of electrodes in sodium-ion batteries as a function of different electrolytes. Despite isostructural similarities, other interactions can have a greater influence on the electrode reaction.

Author contributions

Lina Liers: writing the original draft, visualization, investigation, validation. Lorena Baumgarten: investigation, validation, writing – review & editing. Niels Michaelis: investigation, validation, writing – review & editing. Romy Brüning: investigation, validation, writing – review & editing. Henrik Fritzsch: investigation, validation, writing – review & editing. Jan-Dierk Grunwaldt: funding acquisition, resources, writing – review & editing. Malte Behrens: funding acquisition, resources, writing – review & editing. Sebastian Mangelsen: writing the original draft, visualization, project administration, supervision, formal analysis. The manuscript was written through contributions of all authors. All authors have given approval to the final version of the manuscript.

Conflicts of interest

The authors declare no conflicts of interest.

Data availability

Supplementary information (SI) is available. See DOI: https://doi.org/10.1039/d6ya00228e.

The data that support the findings of this study are available from the corresponding author upon reasonable request.

Acknowledgements

We gratefully acknowledge the State of Schleswig-Holstein for financial support. We would like to thank the Deutsche Forschungsgemeinschaft (DFG, German Research Foundation) for founding the high-resolution scanning electron microscope with an EDX detector – 529613430 (DFGINST 257/717-1 FUGG). The SEM/EDX measurements were carried out by Dr Nicole Pienack and Dennis Egawa from the institute of inorganic chemistry of Kiel University, for which we would like to express our sincere thanks. Furthermore, we would like to thank Dr Sandra Hansen for the loan of the optical cell. The authors acknowledge the CAT-ACT beamline at the KIT Light Source for providing beamtime and the instruments, specifically Dr Anna Zimina for performing XAS measurements. We would further like to thank Maren Rassmussen for the DTA-TG measurements and Dr Tobias Engesser for the help with the IR spectroscopy analysis. The authors thank Prof. Dr Felix Tuczek for providing the resources for the UV/Vis measurements.

References

1 M. L. Divya, Y.-S. Lee and V. Aravindan, *ACS Energy Lett.*, 2021, **6**, 4228–4244.
2 G. A. Ferrero, G. Åvall, K. Janßen, Y. Son, Y. Kravets, Y. Sun and P. Adelhelm, *Chem. Rev.*, 2025, **125**, 3401–3439.
3 Y. Sun, G. Åvall, S.-H. Wu, G. A. Ferrero, A. Freytag, P. B. Groszewicz, H. Wang, K. A. Mazzio, M. Bianchini, V. Baran, S. Risse and P. Adelhelm, *Nat. Mater.*, 2025, **24**, 1441–1449.
4 J. Park, S. J. Kim, K. Lim, J. Cho and K. Kang, *ACS Energy Lett.*, 2022, **7**, 3718–3726.
5 L. Lyu, Y. Yi and Z.-L. Xu, *Batteries Supercaps*, 2025, **8**, e202400521.
6 Y. Son, G. Åvall, G. A. Ferrero, A. I. Freytag, I. Escher, K. A. Janßen, M. Jauregui, D. Saurel, M. Galceran and P. Adelhelm, *Batteries Supercaps*, 2024, **7**, e202300506.
7 A. Leblanc-Soreau, M. Danot, L. Trichet and J. Rouxel, *Mater. Res. Bull.*, 1974, **9**, 191–197.
8 G. Alvarez Ferrero, G. Åvall, K. A. Mazzio, Y. Son, K. Janßen, S. Risse and P. Adelhelm, *Adv. Energy Mater.*, 2022, **12**, 2202377.
9 W. B. Johnson and W. L. Worrell, *Synth. Met.*, 1982, **4**, 225–248.
10 M. S. Whittingham, *Prog. Solid State Chem.*, 1978, **12**, 41–99.
11 M. S. Whittingham and F. R. Gamble, *Mater. Res. Bull.*, 1975, **10**, 363–371.
12 L. Liers, L. Mereacre, H. Li, J. Mickenbecker, M. Knapp, S. Indris, M. Behrens and S. Mangelsen, *Inorg. Chem.*, 2025, **64**, 18045–18061.
13 J. L. Kaufman, J. Vinckevičiūtė, S. Krishna Kolli, J. Gabriel Goiri and A. Van Der Ven, *Philos. Trans. R. Soc., A*, 2019, **377**, 20190020.
14 J. Rouxel, *Physica B+C*, 1980, **99**, 3–11.
15 L. S. Ramsdell, *Am. Mineral.*, 1947, **32**, 64–82.
16 E. A. Marseglia, *Int. Rev. Phys. Chem.*, 1983, **3**, 177–216.
17 R. H. Friend and A. D. Yoffe, *Adv. Phys.*, 1987, **36**, 1–94.
18 J. A. Wilson and A. D. Yoffe, *Adv. Phys.*, 1969, **18**, 193–335.
19 D. L. Greenaway and R. Nitsche, *J. Phys. Chem. Solids*, 1965, **26**, 1445–1458.
20 K. Terashima and I. Imai, *Solid State Commun.*, 1987, **63**, 315–318.
21 A. R. Beal and S. Nulsen, *Philos. Mag. B*, 1981, **43**, 965–983.
22 A. Zimina, K. Dardenne, M. A. Denecke, D. E. Doronkin, E. Huttel, H. Lichtenberg, S. Mangold, T. Pruessmann, J. Rothe, T. Spangenberg, R. Steininger, T. Vitova, H. Geckeis and J.-D. Grunwaldt, *Rev. Sci. Instrum.*, 2017, **88**, 113113.
23 B. Ravel and M. Newville, *J. Synchrotron Radiat.*, 2005, **12**, 537–541.
24 F. A. S. Al-Alamy, A. A. Balchin and M. White, *J. Mater. Sci.*, 1977, **12**, 2037–2042.
25 K. Momma and F. Izumi, *J. Appl. Crystallogr.*, 2011, **44**, 1272–1276.
26 A. A. Coelho, J. S. O. Evans and J. W. Lewis, *J. Appl. Crystallogr.*, 2016, **49**, 1740–1749.

© 2026 The Author(s). Published by the Royal Society of Chemistry

27 V. Aravindan, J. Gnanaraj, S. Madhavi and H.-K. Liu, *Chem. – Eur. J.*, 2011, **17**, 14326–14346.
28 Z. Li, L. Wang, X. Huang and X. He, *Adv. Funct. Mater.*, 2024, **34**, 2408319.
29 O. V. Bushkova, T. V. Yaroslavtseva and Yu. A. Dobrovolsky, *Russ. J. Electrochem.*, 2017, **53**, 677–699.
30 A. H. Thompson, *J. Electrochem. Soc.*, 1979, **126**, 608.
31 W. R. McKinnon and R. R. Haering, in *Modern Aspects of Electrochemistry*, ed. R. E. White, J. O. Bockris and B. E. Conway, Springer US, Boston, MA, 1983, vol, 15, pp. 235–304.
32 B. E. Warren, *Phys. Rev.*, 1941, **59**, 693–698.
33 Q. Liu, F. Wu, D. Mu and B. Wu, *Phys. Chem. Chem. Phys.*, 2020, **22**, 2164–2175.
34 G. Yoon, H. Kim, I. Park and K. Kang, *Adv. Energy Mater.*, 2017, **7**, 1601519.
35 J. Park, Z.-L. Xu and K. Kang, *Front. Chem.*, 2020, **8**, 432.
36 Y.-K. Liu, C.-Z. Zhao, J. Du, X.-Q. Zhang, A.-B. Chen and Q. Zhang, *Small*, 2023, **19**, 2205315.
37 K. Xu, *Chem. Rev.*, 2014, **114**, 11503–11618.
38 W. Xu, Y. Wu, S. Xi, Y. Wang, Y. Wang, Y. Ke, L. Ding, X. Wang, J. Yang, W. Zhang, K. P. Loh, F. Ding, Z. Liu and M. Chhowalla, *Nat. Synth.*, 2025, **4**, 327–335.
39 C.-H. Lin, M. Topsakal, K. Sun, J. Bai, C. Zhao, E. Dooryhee, P. Northrup, H. Gan, D. Lu, E. Stavitski and Y. Karen Chen-Wiegart, *J. Mater. Chem. A*, 2020, **8**, 12339–12350.
40 M. Wang and Z. Feng, *Curr. Opin. Electrochem.*, 2021, **30**, 100803.
41 S. Saha, G. Assat, M. T. Sougrati, D. Foix, H. Li, J. Vergnet, S. Turi, Y. Ha, W. Yang, J. Cabana, G. Rousse, A. M. Abakumov and J.-M. Tarascon, *Nat. Energy*, 2019, **4**, 977–987.
42 P. Moreau, G. Ouvrard, P. Gressier, P. Ganal and J. Rouxel, *J. Phys. Chem. Solids*, 1996, **57**, 1117–1122.

© 2026 The Author(s). Published by the Royal Society of Chemistry